Supporting Information

Umitsu et al. 10.1073/pnas.0905270106

SI Text

Discussion

Comparison with Enzymes Catalyzing Aminoalkyl Group Transfer. Spermidine synthase (SPDS), which is also referred to as putrescine aminopropyltransferase (PAPT), catalyzes a similar reaction to TYW2. SPDS transfers the aminopropyl group from decarboxylated AdoMet (dcAdoMet) to putrescine, to form spermidine. The amino acid sequence of SPDS suggests that the enzyme also belongs to the class-I MTase superfamily. The crystal structure of SPDS revealed that the overall structure of SPDS actually contains the class-I MTase fold, but dcAdoMet is bound to SPDS in a slightly different manner from those observed in the bona fide MTases (1, 2). In SPDS, the "M cavity" is constricted by the conserved Asp residue and cannot accommodate the aminopropyl group of dcAdoMet (Fig. S6*A*). Consequently, the aminopropyl group of dcAdoMet is oriented in the same direction as the methyl group of AdoMet in the bona fide MTases, which enables the transfer of the aminopropyl group, instead of the methyl group, to the substrate. Interestingly, the recognition mechanism of the cofactor in SPDS is very similar to that in TYW2 (Fig. S6). Therefore, it is likely that the conserved Asp residue in the "M cavity" of SPDS plays a similar role to the His/Tyr residue in the "M cavity" of TYW2, which makes the AdoMet binding mode suitable for the acp-group transfer. It is noteworthy that SPDS shares amino acid sequence similarity to putrescine *N*-methyltransferase (PNMT), which transfers the methyl group of AdoMet to putrescine. These observations suggest that TYW2 and SPDS have convergently evolved from different MTases, Trm5 and PNMT, respectively, to acquire similar cofactor recognition and chemical reaction mechanisms.

In addition, the enzymatic transfer of the acp group from AdoMet is widely observed in various biological processes. For example, the biosynthetic pathways for diphthamide (3), the antibiotic nocardicin (4), the germination inhibitor discadenine (5), nicotianamine (6), and the betaine lipid diacylglyceryl-*O*-4′-(*N*,*N*,*N*,-trimethyl) homoserine (7) are considered to use AdoMet as a source of the acp group. The present crystal structures provide structural insights into the acp-group transfer by these enzymes. Diacylglyceryl-*O*-4′-(*N*,*N*,*N*,-trimethyl) homoserine is a non-phosphorous membrane lipid present in plants and bacteria. Its biosynthetic pathway is initiated by the acp-group transfer from AdoMet to diacylglycerol by BtaA (7). Although the 3D structure of BtaA is unavailable, the BtaA orthologues share weak sequence homology with the members of the class I MTase superfamily, which enabled the identification of the key signature motifs, motifs I and II (8). BtaA contains a conserved bulky residue (Asn or Arg) immediately after motif I, which may form the "M cavity." Therefore, we can speculate that these bulky residues may constrict the "M cavity" of BtaA, allowing the AdoMet-binding mode to facilitate the acp-group transfer.

Chemistry of the acp-Group Transfer by TYW2. The structural comparison of PhTYW2 with SPDS suggests that the acp-group transfer by TYW2 and the aminopropyl-group transfer by SPDS (1, 2) proceed via a similar mechanism. Thus, TYW2 may transfer the acp group through a single-displacement mechanism, in which the inversion of the configuration of the methylene carbon occurs during the nucleophilic attack by carbon C7 in the imG-14 nucleobase.

The nucleophilic attack by aromatic carbon atoms is more difficult than that by polarizable nitrogens and oxygens. Therefore, the methyl group transfer to carbon C5 of pyrimidine usually requires a sophisticated mechanism, in which the nucleobase is first activated by covalent-bond formation between the conserved Cys thiol of the enzyme and carbon C6 of the substrate pyrimidine (9). This covalent-bond formation increases the nucleophilicity of carbon C5 and thereby facilitates the methyl transfer reaction. Although TYW2 also catalyzes the acp transfer reaction to the aromatic carbon atom, the present structures showed no conserved Cys residue near the catalytic site. A previous study on the chemical synthesis of Y base derivatives reported that carbon C7 of the imG-14 base is especially reactive for a Friedel-Crafts reaction (10), suggesting a Y-base-specific tautomerism that increases the nucleophilicity of carbon C7. Therefore, it is likely that the acp transfer reaction to carbon C7 of the imG-14 base proceeds without the formation of a covalent intermediate between the enzyme and the nucleobase, as observed in other *N*- and *O*-MTases.

Materials and Methods

Cloning, Expression, and Purification of Archaeal TYW2 Proteins. The ORF PH0793 was amplified by PCR from the *P. horikoshii* genome and was cloned into the *Nde*I/*Xho*I sites of a modified pET28a vector (Novagen), with the thrombin cleavage site replaced by the PreScission Protease site (GE Healthcare). The protein was overexpressed in *Escherichia coli* BL21-CodonPlus(DE3)-RIL cells (Stratagene). *E. coli* cells were grown to an OD_{600} = 0.6, and then the expression was induced by 0.5 mM isopropyl β-D-thiogalactopyranoside (IPTG), followed by cultivation for 3 h at 37 °C. Cells were harvested by centrifugation, resuspended in buffer (50 mM Tris-HCl, pH 8.0, 300 mM NaCl, 20 mM imidazole, and 5 mM 2-mercaptoethanol), sonicated, and then centrifuged. The supernatant was purified by heat treatment at 65 °C for 15 min, followed by column chromatography on Ni-NTA SuperFlow (Qiagen) and HiTrap Heparin (GE Healthcare). The MJ1557 protein was expressed and purified by using the same protocol as for PH0793, except for an additional purification step on a Superdex200 column (GE Healthcare). The purified proteins were dialyzed against buffer (5 mM Tris-HCl, pH 8.0, 300 mM NaCl, and 1 mM DTT), concentrated, and used for an in vitro modification assay and crystallization. The PhTYW2 mutants were prepared by using the QuikChange method (Stratagene), and the sequences were verified by DNA sequencing. The mutant proteins were purified by using the same protocol as for the wild-type, and used for an in vitro modification assay.

Crystallization. Crystallization was performed at 20 °C by the sitting and hanging drop vapor diffusion methods. Crystals of the PhTYW2-AdoMet and PhTYW2-MeSAdo complexes were grown by mixing 1 μL of the protein solution (10 mg/mL in 5 mM Tris-HCl, pH 8.0, 300 mM NaCl, 1 mM DTT, and 1–3 mM AdoMet or MeSAdo) and 1 μL of the reservoir solution (0.1 M Mes-NaOH, pH 6.0, and 14% PEG10,000). Crystals of the MjTYW2-AdoMet complex were grown by mixing 1 μL of the protein solution (10 mg/mL in 5 mM Tris-HCl, pH 8.0, 300 mM NaCl, 1 mM DTT, and 1–3 mM AdoMet) and 1 μL of the reservoir solution (0.1 M Mes-NaOH, pH 6.5, 0.1 M ammonium sulfate, and 15% PEG5,000). Crystals suitable for analysis were grown within 3 days.

Data Collection and Structure Determination. x-ray diffraction data were collected at 100 K on beamline BL41XU at SPring-8 (Hyogo) and beamline NW12A at PF-AR (Tsukuba). The crystals of PhTYW2 and MjTYW2 were cryo-protected in each reservoir solution supplemented with 30% and 25% PEG400, respectively. Diffraction data were processed using the HKL2000 software (HKL Research). Phases were determined by molecular replacement with the program MOLREP (11), using the deposited structure of the apo-form of PH0793 (PDB ID: 2FRN) as a search model. The initial model of MjTYW2 was improved by the program ARP/wARP (12). All of the models were manually built with the program COOT (13), and were refined with the programs Refmac (14) and PHENIX (15). Data collection and refinement statistics are provided in Table S1. Structural figures were prepared using PyMol (DeLano Scientific; http://www.pymol.org/).

Measurement of the tRNA Modification Activity of Archaeal TYW2 by Mass Spectroscopic Analysis. The yeast TYW2 protein and the tRNA with the imG-14 intermediate, obtained from the ΔTYW2 strain ($tRNA^{Phe}$-imG-14), were prepared as previously reported (16). Reaction mixtures (10 μL), containing 50 mM Tris-HCl (pH 8.0), 0.5 mM DTT, 10 mM $MgCl_2$, 1 mM spermidine, 2 μg $tRNA^{Phe}$-imG-14, and 1.4 μM recombinant yeast TYW2, *P. horikoshii* TYW2, or *M. jannaschii* TYW2 protein, with or without 0.5 mM AdoMet, were incubated for 1 h at 30 °C for the yeast protein, and 50 °C for the archaeal proteins. The $tRNA^{Phe}$ was recovered by TRIzol LS purification (Invitrogen), precipitated by ethanol and then subjected to $RNaseT_1$ digestion to produce the anticodon-containing fragment (ACmUG-mAA[imG-14]AΨm^5CUGp, MW 3980). To analyze the RNA fragments digested by $RNaseT_1$, we devised a system of capillary LC coupled with nanoESI-MS (17). A linear ion trap-orbitrap hybrid mass spectrometer (LTQ Orbitrap XL, Thermo Fisher Scientific) was equipped with a custom-made nanospray ion source, a Nanovolume Valve (Valco Instruments), and a splitless nano HPLC system (DiNa, KYA Technologies). The analyte mixed with TEAA was loaded onto a nano-LC trap column (C18, Φ0.5 × 1.0 mm), desalted, and then concentrated with 0.1 M TEAA (pH 7.0). RNA fragments were eluted from the trap column and directly injected into a C18 capillary column (HiQ Sil; 3 μm C18, 100 Å pore size; Φ0.1 × 100 mm, KYA Technologies). The solvent system consisted of 0.4 M 1,1,1,3,3,3-hexafluoro-2-propanol (HFIP; pH 7.0, adjusted with triethylamine; solvent A) and 0.4 M HFIP in 50% methanol (solvent B), and the samples were chromatographed at a flow rate of 300 nL/min, using a linear gradient of 10%–90% solvent B over 35 min. The chromatographic eluent was sprayed from a sprayer tip attached to the capillary column. The ionization voltage was set to −1.9 kV, and the ions were scanned in the negative polarity mode. The mass spectrum was acquired in the range of *m/z* 600 to 2,000, with a mass resolution of 30,000 (FWHM).

Measurement of the tRNA Modification Kinetics of Archaeal TYW2 by a Radioisotope-Incorporation Assay. The purified yeast TYW2 and PhTYW2 proteins (1 μM) were mixed with 2.5 μM $tRNA^{Phe}$-imG-14, 58 μM AdoMet, and 47 μM [carboxyl-^{14}C] AdoMet (50 mCi/mmol, America Radiolabeled Chemicals, Inc.) in a final reaction volume of 50 μL, in reaction buffer containing 50 mM Tris-HCl (pH 8.0), 0.5 mM DTT, 10 mM $MgCl_2$, and 1 mM spermidine. As a negative control, the reaction mixture without enzyme was used. Reactions were incubated at 30 °C and 50 °C for the yeast and archaeal proteins, respectively. Aliquots (15 μL) were taken at 15, 30, and 60 min, spotted onto Whatman 3MM filters, and precipitated onto the filters with 5% (wt/vol) trichloroacetic acid (TCA). The filters were washed briefly three times, for 15 min three times, and again briefly three times, with 5% TCA at 4 °C. The washed filters were further washed with 100% (vol/vol) ethanol, dried, and then subjected to scintillation counting to determine the amount of [^{14}C]acp group incorporation. Assays performed in triplicate consistently revealed small mean deviations of the determined counts.

1. Korolev S, et al. (2002) The crystal structure of spermidine synthase with a multisubstrate adduct inhibitor. *Nat Struct Biol* 9:27–31.
2. Dufe VT, et al. (2007) Crystal structure of *Plasmodium falciparum* spermidine synthase in complex with the substrate decarboxylated *S*-adenosylmethionine and the potent inhibitors 4MCHA and AdoDATO. *J Mol Biol* 373:167–177.
3. Liu S, et al. (2004) Identification of the proteins required for biosynthesis of diphthamide, the target of bacterial ADP-ribosylating toxins on translation elongation factor 2. *Mol Cell Biol* 24:9487–9497.
4. Reeve AM, Breazeale SD, Townsend CA (1998) Purification, characterization, and cloning of an *S*-adenosylmethionine-dependent 3-amino-3-carboxypropyltransferase in nocardicin biosynthesis. *J Biol Chem* 273:30695–30703.
5. Taya Y, Tanaka Y, Nishimura S (1978) Cell-free biosynthesis of discadenine, a spore germination inhibitor of *Dictyostelium discoideum*. *FEBS Lett* 89:326–328.
6. Higuchi K, et al. (1999) Cloning of nicotianamine synthase genes, novel genes involved in the biosynthesis of phytosiderophores. *Plant Physiol* 119:471–480.
7. Klug RM, Benning C (2001) Two enzymes of diacylglyceryl-*O*-4′-(*N*,*N*,*N*,-trimethyl)homoserine biosynthesis are encoded by *btaA* and *btaB* in the purple bacterium *Rhodobacter sphaeroides*. *Proc Natl Acad Sci USA* 98:5910–5915.
8. Riekhof WR, Andre C, Benning C (2005) Two enzymes, BtaA and BtaB, are sufficient for betaine lipid biosynthesis in bacteria. *Arch Biochem Biophys* 441:96–105.
9. Schubert HL, Blumenthal RM, Cheng X (2003) Many paths to methyltransfer: A chronicle of convergence. *Trends Biochem Sci* 28:329–335.
10. Itaya T, Mizutani A, Takeda M, Shioyama C (1989) Studies towards the synthesis of the fluorescent bases of phenylalanine transfer ribonucleic acids: Synthesis of 7-methylwye isolated from extremely thermophilic archaebacteria. *Chem Pharm Bull (Tokyo)* 37:284–291.
11. Vagin A, Teplyakov A (1997) MOLREP: An automated program for molecular replacement. *J Appl Cryst* 30:1022–1025.
12. Langer G, Cohen SX, Lamzin VS, Perrakis A (2008) Automated macromolecular model building for X-ray crystallography using ARP/wARP version 7. *Nat Protoc* 3:1171–1179.
13. Emsley P, Cowtan K (2004) Coot: Model-building tools for molecular graphics. *Acta Crystallogr D Biol Crystallogr* 60:2126–2132.
14. Murshudov GN, Vagin AA, Dodson EJ (1997) Refinement of macromolecular structures by the maximum-likelihood method. *Acta Crystallogr D Biol Crystallogr* 53:240–255.
15. Adams PD, et al. (2002) PHENIX: Building new software for automated crystallographic structure determination. *Acta Crystallogr D Biol Crystallogr* 58:1948–1954.
16. Noma A, Kirino Y, Ikeuchi Y, Suzuki T (2006) Biosynthesis of wybutosine, a hypermodified nucleoside in eukaryotic phenylalanine tRNA. *EMBO J* 25:2142–2154.
17. Suzuki T, et al. (2007) Mass spectrometric identification and characterization of RNA-modifying enzymes. *Methods Enzymol* 425:211–229.
18. McLuckey SA, Goeringer DE, Glish GL (1992) Collisional activation with random noise in ion trap mass spectrometry. *Anal Chem* 64:1455–1460.
19. Sugawara H, et al. (2009) DDBJ dealing with mass data produced by the second generation sequencer. *Nucleic Acids Res* 37:D16–18.

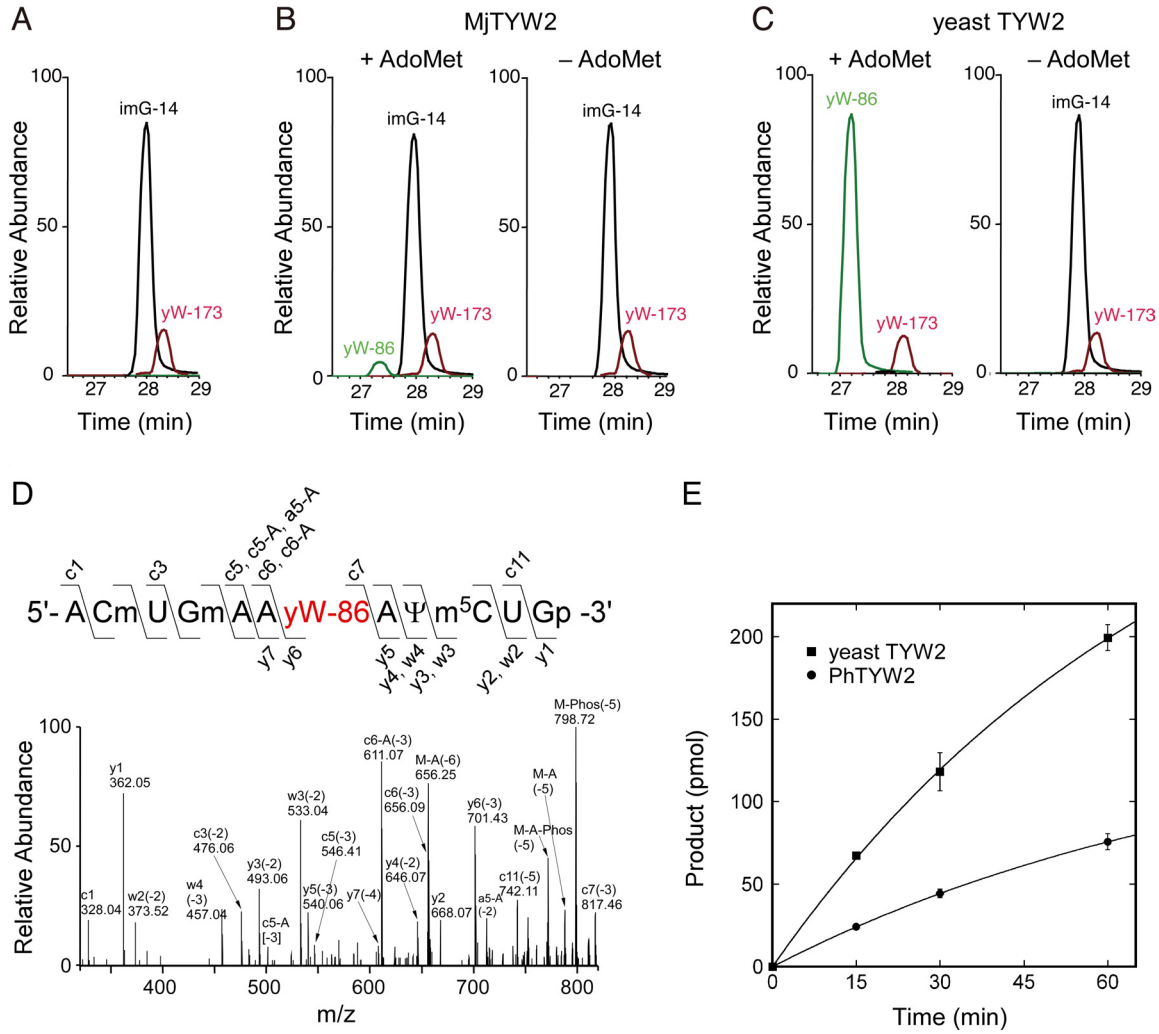

Fig. S1. In vitro reconstitution of yW-86 by recombinant TYW2 proteins. (*A*) RNaseT$_1$-digested yeast tRNA^{Phe} with the imG-14 intermediate (black), obtained from the ΔTYW2 strain, was reacted with recombinant MjTYW2 (*B*) or yeast TYW2 (*C*) in the presence (left panel) or absence (right panel) of AdoMet, and was analyzed by LC/MS. The mass chromatographs for the anticodon-containing fragments harboring imG-14(*m/z* 661, black), yW-86(*m/z* 678, green), and yW-173(*m/z* 664, red) are overlaid. (*D*) Collision-induced dissociation (CID) spectrum of the anticodon-containing fragment of tRNA^{Phe} bearing yW-86, which was reconstituted with recombinant PhTYW2 in the presence of AdoMet. [M-6H]$^{-6}$(*m/z* 679.10) was selected as a precursor mass for CID. The product ions were assigned as described (18). Partial sequences from both termini determined by this spectrum are indicated. ''M'' stands for the parent mass. The charge state of each ion is shown in parentheses. Loss of the adenine base and the phosphate from each ion is described as ''-A'' and ''-Phos,'' respectively. (*E*) Kinetic analysis of the acp-group transfer by PhTYW2 and yeast TYW2. α-carboxyl-^{14}C labeled AdoMet and the imG-14 containing tRNA^{Phe} were incubated at 50 °C with recombinant PhTYW2 (closed circles) and at 30 °C with yeast TYW2 (closed squares), and the incorporation of α-carboxyl-^{14}C into the tRNA^{Phe} was quantified by scintillation counting. Data are represented as mean ± *SE* (*n* = 3).

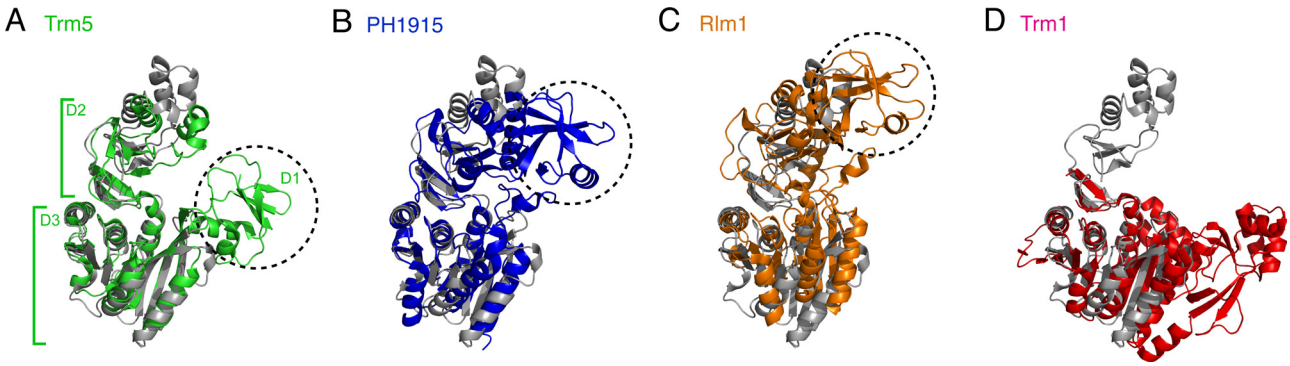

Fig. S2. Superposition of the PhTYW2 structure onto its closely-related MTase structures. The crystal structure of PhTYW2, colored gray, and (*A*) the crystal structure of *M. jannaschii* tRNA(m^1G37) MTase Trm5, colored green (PDB ID 2YX1, Z score = 27.9 with RMSD of 3.9 Å for 249 Cα atoms), (*B*) the crystal structure of *P. horikoshii* putative MTase PH1915, colored blue (PDB ID 2AS0, Z score = 22.9 with RMSD of 3.9 Å for 240 Cα atoms), (*C*) the crystal structure of *E. coli* 23S rRNA(m^5C) MTase Rlm1, colored orange (PDB ID 3C0K, Z score = 21.3 with RMSD of 4.3 Å for 244 Cα atoms), and (*D*) the crystal structure of *P. horikoshii* tRNA(m^2_2G26) dimethytransferase Trm1, colored red (PDB ID 2DUL, Z score = 20.8 with RMSD of 1.9 Å for 180 Cα atoms), are shown in ribbon representations. Dashed circles indicate OB-fold domains.

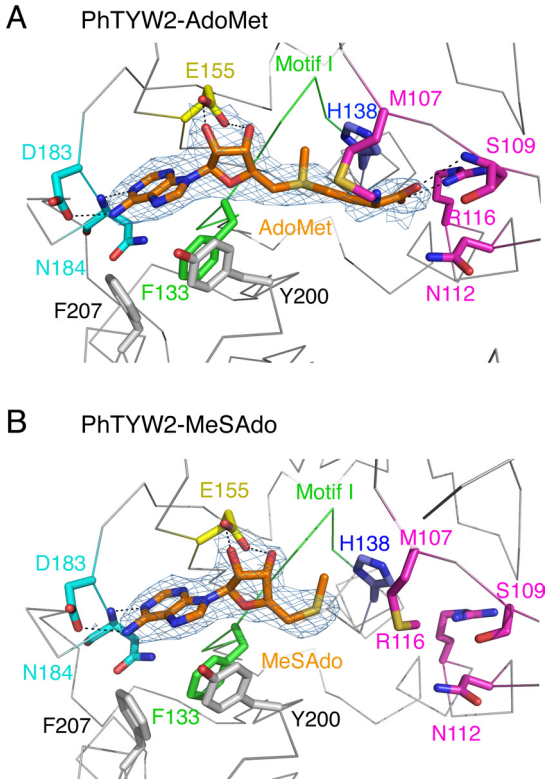

Fig. S3. Electron density maps of cofactors bound to PhTYW2. $2F_o-F_c$ annealed omit maps around cofactors contoured at 1.0 σ are shown. AdoMet (*A*) and MeSAdo (*B*) are shown in stick models and are colored orange. The residues involved in the AdoMet binding are depicted by stick models and are colored as in Fig. 3*A*.

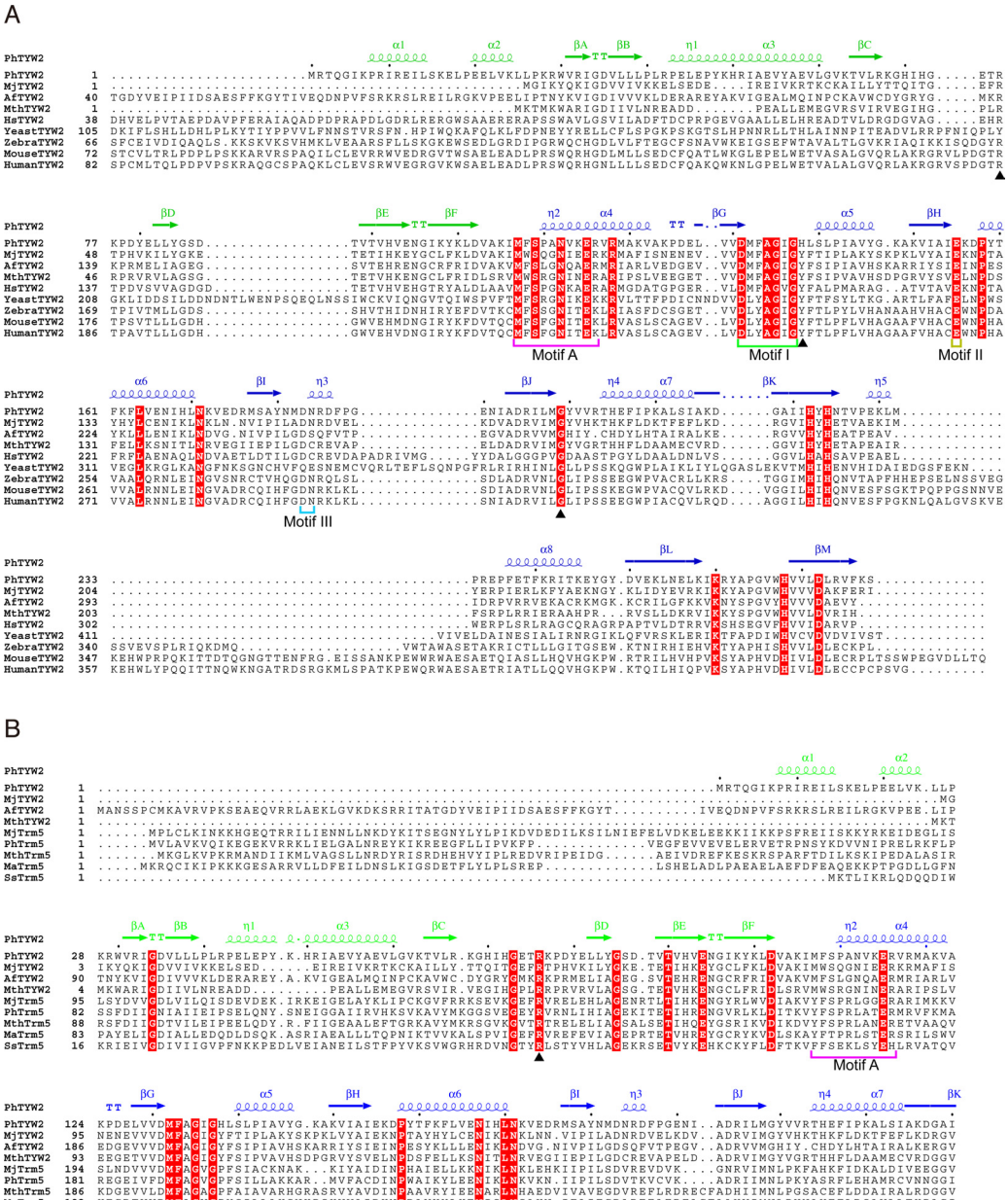

Fig. S4. Amino acid sequence alignments of (*A*) TYW2 homolog proteins and (*B*) archaeal TYW2 and archaeal Trm5 proteins. Abbreviations are as follows: Ph, *Pyrococcus horikoshii*; Mj, *Methanococcus jannaschii*; Af, *Archaeoglobus fulgidus*; Mth, *Methanothermobacter thermautotrophicus*; Hs, *Halobacterium sp.* NRC-1; *Ss*, *Sulfolobus solfataricus*; Yeast, *Saccharomyces cerevisiae*; Zebrafish, *Danio rerio*; Mouse, *Mus musculus*; and Human, *Homo sapiens*. The fully conserved residues are highlighted in red boxes. The PhTYW2 secondary structures for α-helices (denoted as α), β-strands (β), and 3_{10}-helices (η) are shown above the sequences. The N- and C-terminal domains are colored green and blue, respectively. Motifs A, I, II, and III are indicated below the sequences by magenta, green, yellow, and cyan lines, respectively. Residues discussed in the main text are indicated by triangles. The sequences were aligned using the program ClustalW (19), and the figure was generated with the program ESPript (http://espript.ibcp.fr/ESPript/ESPript/).

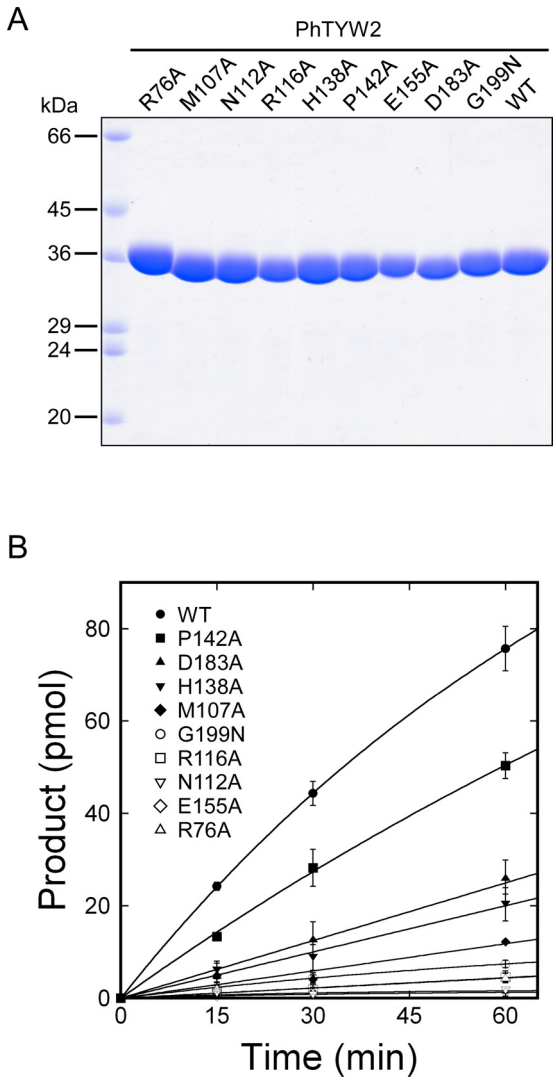

Fig. S5. Mutational analysis of the acp-group transfer by PhTYW2. (*A*) 10% SDS-PAGE analysis of the purified wild-type and mutants of PhTYW2 used for the radioisotope-incorporation assay. The gel was stained with Coomassie Brilliant Blue. (*B*) Kinetic analysis of the acp-group transfer by the wild-type and mutants of PhTYW2. α-carboxyl-^{14}C labeled AdoMet and the imG-14 containing tRNA^{Phe} were incubated at 50 °C with the PhTYW2 proteins, and the incorporation of α-carboxyl-^{14}C into the tRNA^{Phe} was quantified by scintillation counting. Data are represented as mean $\pm$ *SE* ($n = 3$), and are plotted with different symbols.

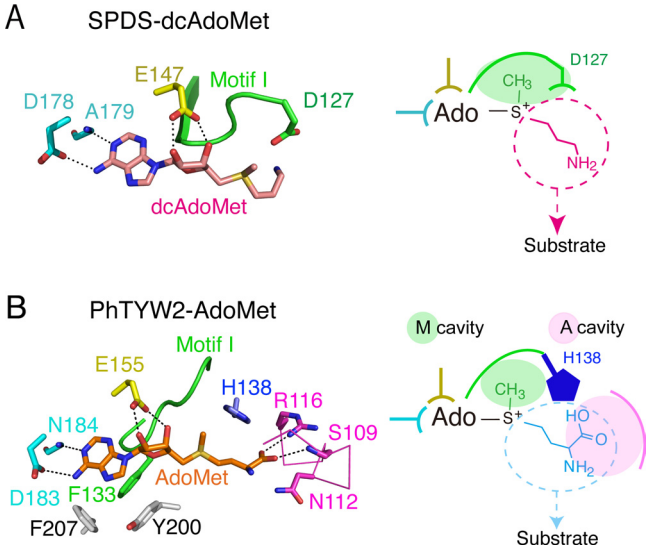

Fig. S6. Structural comparison of the cofactor-binding pockets in (*A*) spermidine synthase (SPDS) with dcAdoMet (PDB ID 2PT6) and (*B*) PhTYW2 with AdoMet. dcAdoMet and AdoMet are colored pink and orange, respectively. Residues involved in the cofactor recognition are shown by stick models (left panels). Interactions are indicated with black dashed lines. Motifs I, II, and III are colored green, yellow, and cyan, respectively. His-138 (B) is colored blue, and the hydrophobic residues that recognize the adenine moiety of AdoMet are colored gray. Schematic diagrams of the cofactor binding pocket are shown in the right panels. The M and A cavities are shown in green and magenta circles, respectively.

Table S1. Data collection statistics

Dataset	PhTYW2 AdoMet	PhTYW2 MeSAdo	MjTYW2 AdoMet
Beamline	SPring-8 BL41-XU	SPring-8 BL41-XU	SPring-8 BL41-XU
Wavelength, Å	1.0000	1.0000	1.0000
Space group	*R*3	*R*3	$P2_12_12_1$
Cell dimensions			
a, Å	131.6	132.6	40.6
b, Å	131.6	132.6	67.8
c, Å	99.4	96.7	113.2
α, °	90	90	90
β, °	90	90	90
γ, °	120	120	90
Resolution, Å	50.0–2.3 (2.38–2.3)	50.0–2.5 (2.59–2.50)	50.0–2.0 (2.07–2.0)
No. of unique reflections	26,936	21,055	19,841
Redundancy	3.8 (2.0)	4.2 (2.6)	4.8 (3.3)
Completeness, %	94.5 (78.2)	96.4 (80.5)	91.8 (72.4)
$I/\sigma(I)$	26.1 (1.6)	31.6 (2.7)	36.2 (7.1)
R_{sym}	0.071 (0.390)	0.066 (0.295)	0.077 (0.226)
Resolution, Å	50.0–2.3	50.0–2.5	50.0–2.0
R_{work}, %	20.5	21.3	21.0
R_{free}, %	24.0	24.7	25.5
σ_A coordinate error, Å	0.33	0.33	0.27
No. of			
Protein atoms	2,163	2,154	1,820
Ligands/ions	27	33	27
Waters	147	54	79
Average *B*-factor, Å^2			
Protein	66.1	65.3	56.4
Ligand/ion	66.5	58.0	65.9
Water	68.8	61.8	56.0
RMSD from ideal values			
Bond lengths, Å	0.009	0.009	0.005
Bond angles, °	1.4	1.2	1.0
Ramachandran plot, %			
Most favored	88.8	87.9	89.3
Allowed	9.9	11.2	10.7
Generously allowed	1.3	0.9	0.0
PDB ID code	3A25	3A26	3A27

The numbers in parentheses are for the last shell. $R_{work} = \Sigma|F_o–F_c|/\Sigma F_o$ for reflections of work set.
$R_{free} = \Sigma|F_o - F_c|/\Sigma F_o$ for reflections of test set.